Talanta 257 (2023) 124361



Contents lists available at ScienceDirect

Talanta

journal homepage: www.elsevier.com/locate/talanta

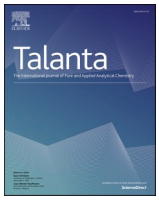



The development of electrochemical DNA biosensor based on poly-L-methionine and bimetallic AuPt nanoparticles coating: Picomolar detection of Imatinib and Erlotinib

Dilek Eskiköy Bayraktepe *, Ceren Yıldız, Zehra Yazan **

Ankara University Faculty of Science Department of Chemistry, Ankara, 06560, Turkey

ARTICLE INFO

Handling Editor: J.-M. Kauffmann

Keywords:
Bimetallic nanoparticles
Electropolymerization
DNA biosensor
Imatinib
Erlotinib
Voltammetry

ABSTRACT

We report on the preparation of a new and simple electrochemical DNA biosensor based on DNA/AuPt/p-L-Met coating on a screen-printed carbon electrode (SPE) and its use in the determination of the cancer therapy agents, Imatinib (IMA) and Erlotinib (ERL). Poly-L-methionine (p-L-Met), gold, and platinum nanoparticles (AuPt) were successfully coated by one-step electrodeposition onto the SPE from a solution containing L-Met, $HAuCl_4$, and H_2PtCl_6. The immobilization of DNA was achieved by drop-casting on the surface of the modified electrode. Cyclic Voltammetry (CV), Electrochemical Impedance Spectroscopy (EIS), Field-Emission Scanning Electron Microscopy (FE-SEM), Energy-Dispersive X-ray Spectroscopy (EDX), and Atomic Force Microscopy (AFM) were used to investigate the morphology, the structure, and the electrochemical performance of the sensor. Experimental factors influencing the coating and DNA immobilization processes were optimized. The peak currents originating from guanine (G) and adenine (A) oxidation of ds-DNA were used as signals to quantify IMA and ERL in the concentration range 2.33–80 nM and 0.032–1.0 nM with the LODs of 0.18 nM and 0.009 nM, respectively. The biosensor developed was suitable for determining IMA and ERL in human serum and pharmaceutical samples.

1. Introduction

Imatinib (IMA), 4-[(4-methyl-1-piperazinyl) methyl]-N-[4-methyl-3-[[4-(3-pyridinyl) 2 pyrimidinyl] amino]-phenyl] benzamide methanesulfonate, is an inhibitor of the tyrosine kinase protein, which inhibits the Bcr-Abl tyrosine kinase. It is used to treat a slow-growing type of cancer of the blood and bone marrow known as chronic myeloid leukemia [1]. Therapeutic doses of the medication of IMA in serum were reported between 0.138 and 3.011 μg/mL for patients [2]. Another tyrosine kinase inhibitor, Erlotinib (ERL), is used to treat a type of lung cancer and pancreatic cancer. Common side effects include rash, diarrhea, myalgia, joint pain, and cough [3]. A decrease in the prescribed doses of these drugs can cause severe adverse reactions. On the other hand, high-dose exposure causes discomfort, such as facial edema, rashes, and itching on the skin [4]. After few weeks of erlotinib therapy, therapeutic doses of ERL in serum was reported as in the range of 0.8–1.25 μg/mL [5]. The quantitative analysis of IMA and ERL in clinical samples is required to keep track of the chemicals in body fluids. Several analytical methods, such as liquid chromatography [6–9], UV-Vis spectroscopy [10,11], and electrochemical methods [12,13], were developed for the quantification of IMA and ERL in urine, pharmaceutical preparations, and also in body fluids.

In recent years, the development of electrochemical biosensors attracted a great deal of attention due to notable characteristics, namely, selectivity, sensitivity, simplicity, rapidity, and low cost [14]. The active layers on the surface of these sensing systems contain a biological recognition component, such as nucleic acids, antibodies, enzymes, proteins etc., that reacts with the target analyte selectively and generates an electrical signal associated with the concentration of the analyte [15,16]. Among these, electrochemical DNA biosensors (EDBs) were found to be effective in developing new procedures to identify many specific molecules, such as anti-cancer drugs [17] and metals [18], by immobilizing nucleic acid (single-stranded or double-stranded DNA) onto the electrode surface. Surfaces prepared in this way are called electrochemical converters [19]. The design and application of the EDBs are generally based on two procedures: The hybridization of the nucleic

* Corresponding author.
** Corresponding author.
E-mail addresses: dilekeskikoy@gmail.com, deskikoy@ankara.edu.tr (D. Eskiköy Bayraktepe), zdurmus@science.ankara.edu.tr (Z. Yazan).

https://doi.org/10.1016/j.talanta.2023.124361
Received 26 December 2022; Received in revised form 9 February 2023; Accepted 12 February 2023
Available online 13 February 2023
0039-9140/© 2023 Elsevier B.V. All rights reserved.

acid strand on the surface of the electrode. This procedure usually involves observing a current response, based on a complementary matching recognition event, under controlled potential [20]. The other procedure is based on the interaction between DNA and drugs and monitoring the drug's redox peak current or adenine/guanine oxidation peak current over the surface of the electrode. This interaction causes a decrease in the peak currents [21]. In this type of biosensor, the working electrodes are generally used as a converter. The electrode materials may be carbon- or metal-based. Carbon-based working electrodes offer a wider potential range than metal-based ones. Glassy carbon, carbon paste, pencil graphite, and screen-printed carbon electrodes (SPEs) are different forms of carbon used for this purpose. Among them, SPEs are well-established materials for the preparation of biosensors. They have reduced the cost of production and sample size. Besides, they are fast, portable, highly selective and sensitive [22]. However, if SPEs are used without a further treatment, several problems arise due to over potential and low redox current. To overcome these drawbacks, the surfaces are functionalized with various biocompatible materials such as metal nanoparticles, carbon nanotubes, biopolymers, and clay minerals [23–26]. Metal nanoparticles have excellent properties, providing high surface area, increased catalytic activity, and a high signal-to-noise ratio. Significantly, Bimetallic nanomaterials are good candidates for surface modification, because they provide useful catalytic features, higher electrical conductivity, synergistic effects, and more active sites, compared to the monometallic ones [27–29].

AuPt bimetallic nanoparticles are common materials for surface treatment. They increase the electroanalytical performance of the sensor by imparting unusual catalytic effects. The use of these noble metals is also preferred for the reason of being biocompatible and always available for conjugation with biomolecules such as proteins, enzymes, DNA, and amino acids [30].

The amino acid, L-methionine (L-Met), that bears the –SH group may form a conductive polymer on the electrode surface and increase the surface area by making the surface more porous, thus enabling nanoparticles to adhere to the surface more efficiently. In addition, the surfaces containing polymer matrices such as p-L-Met provide a suitable environment for immobilizing nucleic acids since p-L-Met contains –COOH groups. The incorporation of nano-sized metals into the p-L-Met film was found to enhance signal resolution [18].

In the current study, a new electrochemical DNA biosensor based on AuPt bimetallic nanoparticles and p-L-Met modified SPE sensor (DNA/AuPt/p-L-Met/SPE) was developed and used for the determination of two tyrosine kinase inhibitors, IMA and ERL. To our literature knowledge, bimetallic and polyaminoacid-based electrochemical DNA biosensors have never been used to determine IMA and ERL. This research offers the development of an electrochemical DNA biosensor using AuPt/p-L-Met composites to determine IMA and ERL quickly for the first time.

To this end, the ds-DNA was immobilized by drop-casting onto SPE via adsorption. Au and Pt nanoparticles were obtained by the electroreduction of $HAuCl_4$ and H_2PtCl_6 on the electrode surface. Electrodes of optimum performance were obtained by changing the concentrations of $HAuCl_4$, H_2PtCl_6, L-Met, and the number of coating cycles. The DNA concentrations and the interaction time with the analytes were optimized by trial. The oxidation CV signals of guanine and adenine on the DNA molecule were used during the optimization trials. The interference of common compounds and reproducibility of the DNA biosensors were also investigated. The biosensor developed was applied to detecting IMA and ERL in human serum and pharmaceutical samples containing known amounts of IMA and ERL.

2. Experimental

2.1. Chemicals and solutions

Imatinib mesylate, erlotinib hydrochloride, L-methionine, tetra chloroauric acids ($HAuCl_4$), and Chloroplatinic acid (H_2PtCl_6), the sodium salt of double-stranded calf thymus DNA (ds-DNA), human (male, AB) plasma serum, potassium ferricyanide $K_3[Fe(CN)_6]\cdot 3H_2O$, potassium ferrocyanide $K_4[Fe(CN)_6]\cdot 3H_2O$, phosphoric acid (H_3PO_4), sodium hydroxide (NaOH), acetic acid (CH_3COOH), ethanol (CH_3CH_2OH), and methanol(CH_3OH) were purchased from Sigma-Aldrich Company (from St. Louis, Missouri, United States). Each material was of analytical grade purity. The stock solutions of ds-DNA were prepared by dissolving ds-DNA sodium salt in double-distilled water. 10.0 mM $HAuCl_4$, 10.0 mM H_2PtCl_6, and 10.0 mM methionine stock solutions were prepared by dissolving appropriate amounts of solids in known volumes of distilled water. 1.0 mM stock solutions of IMA and ERL were prepared by dissolving estimated amounts of solids in methanol. All stock solutions were kept at +4 °C in the fridge until assay.

2.2. Equipment

All electrochemical measurements were carried out using PalmSens *4* potentiostat/galvanostat (from Holland) with PSTrace 5.9 software. Screen-printed carbon electrodes (SPE, DRP-C110) from Dropsens Metrohm were used as a three-electrode (working, reference, and auxiliary electrodes) system. The device connection of SPEs was provided with a connector supplied by Palmsens Company. The solutions prepared during all experimental studies were prepared with double-distilled water obtained from the mpMINIpure water distillation system. pH measurements during the experimental studies were measured with a HANNA HI2211 model pH/ORP meter. The pH meter calibration was performed at room temperature with commercial buffer solutions of pH 4.0, 7.0, and 10.0. The materials were weighed with a Shimadzu AUW220D model precision balance with 0.01 mg sensitivity. Weight lab Instruments WN-2800 model vortex mixer was used to mix the prepared solutions in a small Eppendorf.

The surface morphology of biosensors was investigated with Field Emission Scanning Electron Microscope (FE-SEM) Quanta FEG 250 model (FEI, Holland). FE-SEM was examined using an electron acceleration voltage of 20 KeV. Before analysis, the samples were mounted on an aluminum stab using double-sided carbon tape and coated with a 10 nm thick gold film using a sputter coater. The polymer film thicknesses of the sensors were examined by Park Systems, XE-100E model Atomic Force Microscopy (AFM) with NC-AFM head mode, 0.5 Hz scan rate, and 19 nm amplitude.

2.3. Fabrication of the DNA/AuPt/p-L-Met/SPE biosensor

AuPt/p-L-Met/SPE sensor was prepared by concurrent electrodeposition and electropolymerization processes with the CV method. To this end, the bare SPE surface was subjected to CV cycles in a solution containing 0.5 mM $HAuCl_4$, 0.5 mM H_2PtCl_6, and 10.0 mM L-methionine in 0.1 M phosphate buffer solution (PBS), pH 4.3. CV cycles were carried out within the potential scan range, (−0.6)-(+1.5) V for 15 subsequent CV cycles at a scan rate of 100.0 mV/s (Supplementary file, Fig. S1) [18, 31]. To immobilize ds-DNA at AuPt/p-L-Met/SPE electrode surface, 6.0 μL of 1000 ppm stock ds-DNA solution was drop cast onto the surface of the modified SPE electrode, and the surface was left to dryness for 4 h at room temperature.

Fabrication steps for biosensors are illustrated in Scheme 1.

2.4. Preparation of real samples

2.4.1. Pharmaceutical tablet samples

Glivec® tablets labeled as containing 400 mg imatanib, cellulose microcrystalline, crospovidone, hypromellose, magnesium stearate, colloidal anhydrous silica, iron oxide, macrogol and talc and Tarceva® tablets as containing 100 mg erlotinib, lactose monohydrate, hypromellose, hydroxypropyl cellulose, magnesium stearate, microcrystalline cellulose, sodium starch glycolate, sodium lauryl sulfate and titanium

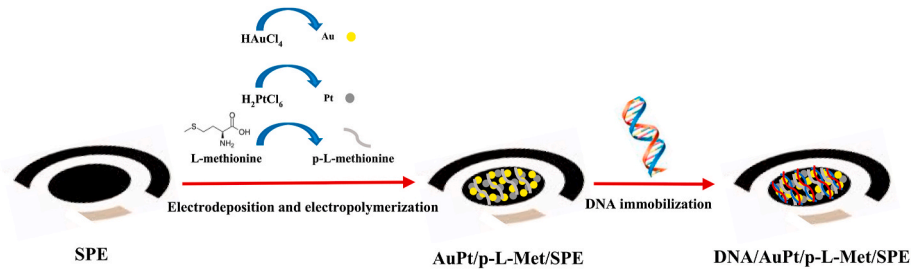

Scheme 1. Fabrication of DNA/AuPt/p-L-Met/SPE biosensor.

dioxide were used to assess the applicability of the biosensor. Three of these tablets were weighed, the average tablet mass was calculated, and then they were crushed into powder in a mortar. A portion of the crushed powder corresponding to one average tablet was weighed and put into a flask, dissolved with methanol, and kept in the refrigerator at +4 °C for 24 h to precipitate insoluble excipients. Appropriate aliquots of these stock tablet solutions were taken, and assay solutions were prepared with 1.0 M acetate buffer (pH 4.8). Then, DPV oxidation signals of A and G were recorded using the DNA/AuPt/p-L-Met/SPE.

2.5. Recovery studies with biological samples

Recovery studies were performed using a commercial human serum sample to test the accuracy of the DNA/AuPt/p-L-Met/SPE biosensor with biological samples. For this purpose, 20.0 μL of human serum stored at −20 °C was dissolved at room temperature and mixed with a solution containing IMA or ERL, and then pH 4.8 acetate buffer was added to the solution, and the total volume was completed to 1.5 mL. Then, the DPV responses of the biosensor were recorded and evaluated using calibration graphs. Recovery tests were carried out by adding known amounts of the analytes to the analyzed serum sample. Recovery of the analytes were assessed using the regression equation provided from the serum calibration plots.

3. Results and discussion

3.1. Preparation of the biosensor

The fabrication procedure of AuPt/p-L-Met/SPE and related voltammograms are given in Section 2.3 and Fig. S1, respectively. As seen in Fig. S1, the L-Met oxidation peak was observed at about +1.4 V. After the second cycle, the peak potential shifted to more negative potentials, and the peak current tended to decrease. These changes in the L-Met peak are probably due to a polymer membrane covering the electrode surface, and the AuPt bimetallic nanoparticles are deposited simultaneously [18,31,32]. The oxidation peak in the second cycle at about +0.8 V and the reduction peak at about −0.1 V belong to the classical oxidation and reduction of gold [33]. Likewise, the reduction peak at about +0.1 V is thought to belong to the reduction of platinum [29,33,34]. As seen in Fig. S1, the increase in the number of cycles shifts the oxidation peak of L-Met to less positive potentials (overall 20.0 mV), and the peak current gradually decreases. The characteristic peaks of Au and Pt increase in the same period. These results showed that L-Met, AuNPs, and PtNPs were co-deposited on the SPE surface to form AuPt/p-L-Met/SPE sensor [18,31]. Then, ds-DNA was immobilized at AuPt/p-L-Met/SPE electrode surface.

3.2. Characterization of the modified biosensor

Surface characterizations (electrode shape, size, and electrode gap) play a crucial role in evaluating electrode materials. The surface morphology of modified electrodes was investigated by the FE-SEM method. FE-SEM images of SPE (a), p-L-Met/SPE (b), AuPt/p-L-Met/SPE (c), and DNA/AuPt/p-L-Met/SPE (d) are shown in Fig. 1. Fig. 1a shows that the bare SPE has a rough and uniform surface structure. After the electropolymerization of p-L-Met on the bare SPE (Fig. 1b), changes in the appearance of the surface occur, which indicates that L-Met polymerization did take place. Fig. 1c represents the surface of AuPt/p-L-Met/SPE, which displays scattered, nearly spherical AuPt nanoparticles. The metallic nanoparticles are also visible on the FE-SEM image of the DNA/AuPt/p-L-Met/SPE surface (Fig. 1d).

Fig. 1e and f shows the EDX spectra obtained from AuPt/p-L-Met/SPE and DNA/AuPt/p-L-Met/SPE biosensor surfaces. The images confirm the formation of AuPt/p-L-Met on the surface of the electrode and the immobilization of ds-DNA. In Fig. 1e, the characteristic peaks of the Au, Pt, S, and O confirm the existence of AuPt/p-L-Met on the surface of the electrode. In the case of DNA/AuPt/p-L-Met/SPE, the signal attributed to P was also observed (Fig. 1f), indicating that the DNA was immobilized to the sensor surface.

The 3D AFM images of SPE, AuPt/p-L-Met/SPE, and DNA/AuPt/p-L-Met/SPE) were given in Fig. 2. The average maximum and minimum height data in 3D images were measured. For comparison, the film thickness of the AuPt/p-L-Met/SPE surface was approximately 70 nm. After the DNA immobilization on this surface, the thickness was approximately 86 nm. These data reveal that the surface area of SPE increases with modifications.

3.3. Electrochemical characterization of DNA/AuPt/p-L-Met/SPE biosensor

The electrochemical characterization of the fabricated biosensor was performed by CV and EIS methods using 5.0 mM Fe $(CN)_6^{3-/4-}$ solution as a probe. 5.0 mM Fe $(CN)_6^{3-/4-}$ solution was prepared in 0.1 M KCl. The CV voltammograms obtained with SPE, AuPt/p-L-Met/SPE, and DNA/AuPt/p-L-Met/SPE are shown in Fig. 3a. The anodic and cathodic peak potential differences (ΔE_p) of Fe $(CN)_6^{3-/4-}$ on different sensor surfaces were also given in Table S1. According to Fig. 3a and Table S1, the lowest anodic and cathodic potential difference value (ΔE_p) with the highest anodic (i_p^a) and cathodic (i_p^c) currents were recorded on the AuPt/p-L-Met/SPE sensor surface. These data show that AuPt/p-L-Met/SPE sensor is of good performance. When this sensor surface was coated with DNA, the redox probe's anodic and cathodic currents decreased, and the ΔE_p value increased by 20 mV (Table S1). This is attributed to the ds-DNA on the electrode blocking the electron transfer process [35] and also be attributed to the repulsion effect between the negatively charged redox probe and the ds-DNA [36].

EIS was also used as an efficient technique to monitor the interface properties of modified electrodes during modifications. Nyquist diagrams at unmodified SPE and AuPt/p-L-Met/SPE with 5.0 mM $[Fe(CN)_6]^{3-/4-}$ probe solution were shown in Fig. 3. Fig. 3b represents the electrochemical impedance of bare SPE electrode (R_{ct} = 0.413 kΩ). R_{ct} value reduces remarkably to 0.157 kΩ with AuPt/p-L-Met/SPE. This indicates that the rate of electron transfers on the modified electrode surface increases. The dsDNA-immobilized electrode (green curve) showed an increase in the R_{ct} value (0.350 kΩ). This may be attributed to ds-DNA's non-conductivity; redox probe ions are hindered from

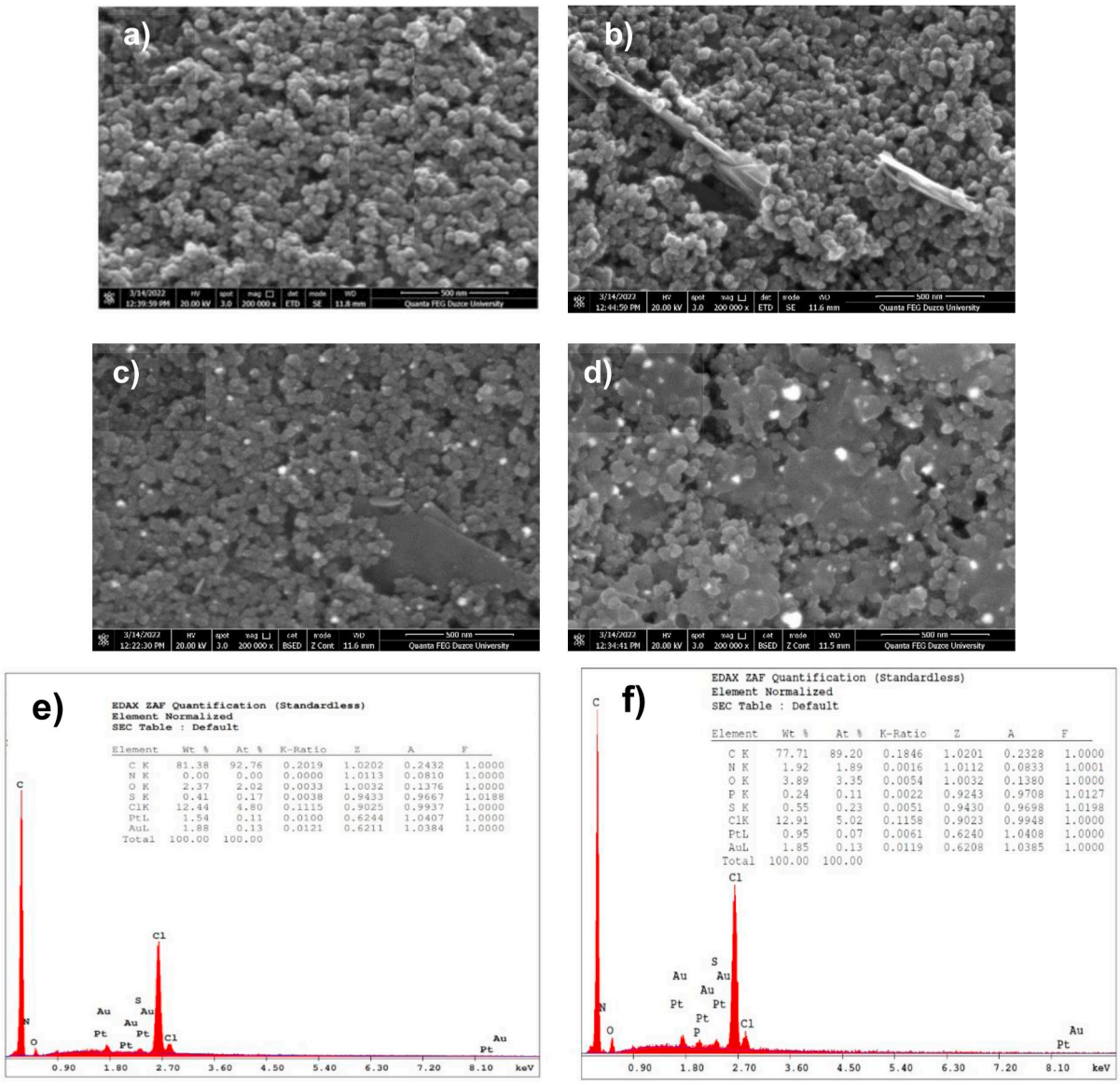

Fig. 1. The SEM images of **a)** bare SPE, **b)** p-L-Met/SPE, **c)** AuPt/p-L-Met/SPE, **d)** DNA/AuPt/p-L-Met/SPE at 20,000 KX and EDX spectrums of **e)** AuPt/p-L-Met/SPE and **f)** DNA/AuPt/p-L-Met/SPE.

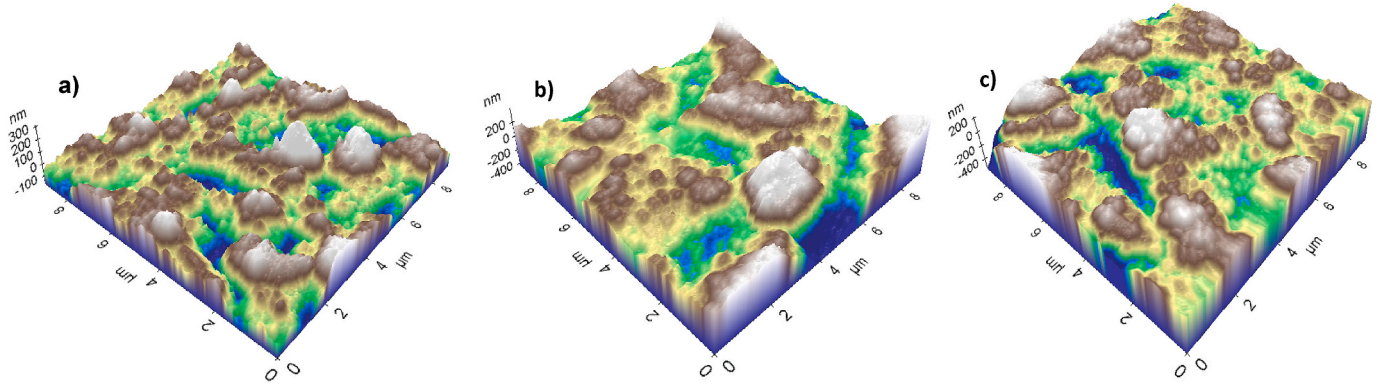

Fig. 2. 3D-AFM images of **a)** SPE, **b)** AuPt/p-L-Met/SPE, and **c)** DNA/AuPt/p-L-Met/SPE (9.09 μm × 9.09 μm).

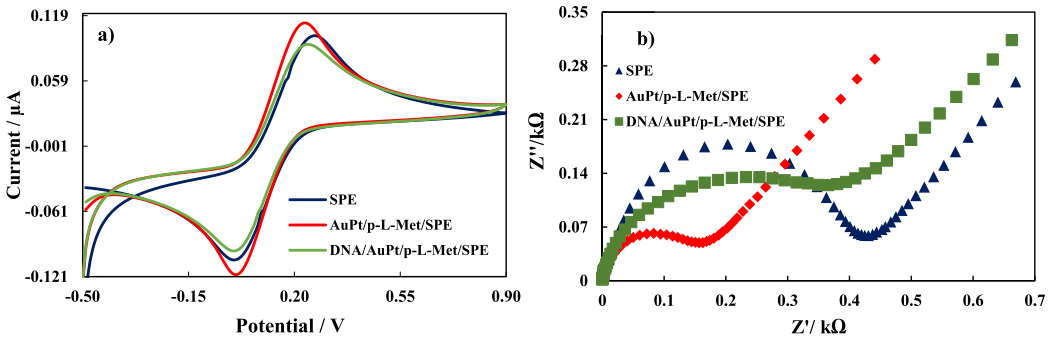

Fig. 3. a) Cyclic voltammograms **b)** Nyquist diagrams of different SPE sensors in 0.1 M KCl solution containing 5.0 mM of $[Fe(CN)_6]^{3-/4-}$ at a scan rate of 0.05 Vs^{-1}.

reaching the electrode and repulsion effect between the negatively charged redox probe and the ds-DNA.

3.4. The comparison of ds-DNA signals with electrodes of different modifications

The electrochemical oxidation of A and G at DNA/SPE (Fig. 4, green line), DNA/Au/p-L-Met/SPE (Fig. 4, orange line), DNA/Pt/p-L-Met/SPE (Fig. 4, blue line), and DNA/AuPt/p-L-Met/SPE (Fig. 4, red line) were studied in acetate buffer solution (0.5 M ABS pH 4.8). As seen in Fig. 4, the oxidation signals of A and G with bare DNA/SPE electrode display broad oxidation peaks with (E_p(G): +0.83 V, i_p^a(G): 0.55 µA and E_p(A): +1.07 V, i_p^a(A): 0.79 µA) which indicates a slow oxidation transfer kinetics for G and A. When the electrode surface was modified with AuPt/p-L-Met, and then with DNA, the oxidation of G and A indicated sharp anodic peaks at 0.82 V and 1.07 V, respectively, and increases occurred in the intensity of the anodic peaks (3.5-folds for G and 2-folds for A).

3.5. Optimization of experimental conditions for the preparation of the biosensor

In order to obtain the highest performance, the concentrations of $HAuCl_4$, H_2PtCl_6, L-Met, and ds-DNA, as well as the number of cycles for CV coatings and scan rate, were optimized. The concentrations of L-Met were changed between 3.0 and 15.0 mM with $HAuCl_4$ and H_2PtCl_6 concentrations fixed at 0.5 mM. After the coating process of each electrode, ds-DNA immobilization was applied. DPV plots were obtained with each electrode immersed in ABS buffer solution (pH 4.8), and the peak currents corresponding to G and A of the ds-DNA were recorded. The results showed that the anodic peak currents of G and A increased to the concentration of L-Met up to 10 mM. A decrease in anodic peak currents was observed with higher concentrations, and the optimum L-Met concentration was selected 10.0 mM (Fig. S2). To optimize the concentrations of $HAuCl_4$ and H_2PtCl_6, the five different concentrations in the range 0.1 mM–1.0 mM were taken for trial with a fixed concentration of L-Met (10 mM). The highest anodic peak current was observed when the mixture contained 0.5 mM $HAuCl_4$ and H_2PtCl_6 (Figs. S3a and b). At concentrations higher than 0.5 mM, the peak current tends to decrease.

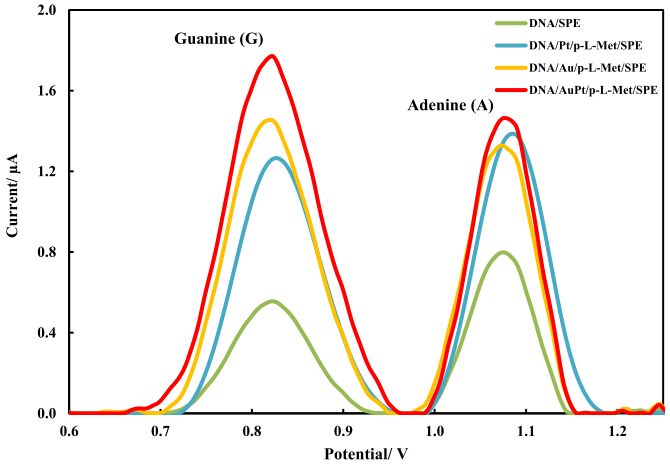

Fig. 4. DPV responses G and A on DNA biosensor surfaces in ABS, pH 4.8 (E_{step}: 0.005 V, t_{pulse}: 0.07 s, scan rate: 0.025 V/s) DNA/SPE (green line), DNA/Au/p-L-Met/SPE (orange line), DNA/Pt/p-L-Met/SPE (blue line), and DNA/AuPt/p-L-Met/SPE (red line).

The effect of the number of coating CV-cycles and scan rate parameters were also investigated in a phosphate buffer solution medium (pH 4.3) containing 0.5 mM $HAuCl_4$ and 0.5 mM H_2PtCl_6, and 10.0 mM L-Met. The number of cycles was changed between 5 and 25 with increments of 5 cycles (Figs. S4a and b). As seen in Fig. S4a, the oxidation peak currents of ds-DNA are almost the same and not influenced by cycling up to 10 cycles, and the currents were suddenly increased at 15 cycles. After 15 cycles, the oxidation peak currents decreased significantly with repetitive cycles. This can be attributed to the fouling of the electrode with increasing cycles after 15 trials.). Similarly, the electrode surface was coated by changing the scan rate in 50.0–175 mV/s with increments of 25 mV/s. The best scan rate was 100 mVs^{-1} (Fig. S4b).

The different concentrations of ds-DNA were used to obtain the maximum A and G signals. The concentration of the DNA solution (6.0 µL) dropped on the surface was changed in the range 50–2000 ppm, and the obtained results showed that A and G signals fluctuated with increasing ds-DNA concentration up to 1000 ppm and decreased at concentrations beyond 1000 ppm (Fig. S5). Therefore, 1000 ppm ds-DNA concentration was chosen as the optimum concentration.

3.6. Optimization and calibration studies for the quantitative analysis of IMA and ERL

IMA and ERL interaction times with the DNA on the electrode surface were optimized to obtain the lowest DPV signals of A and G (Fig. S6). For this purpose, 0.01 µM IMA and ERL solutions were dropped onto the biosensor surface, and the interaction times were changed in the range of 0–240 s. The recorded DPV voltammograms of A and G were evaluated, and the best interaction time for IMA and ERL was selected as 60 s and 120 s, respectively.

After setting the biosensing system to the conditions found by optimization, the oxidation current signals of A and G were evaluated by changing the IMA and ERL concentrations in the range 0.1–80.0 nM and 0.01–1.0 nM, respectively. As shown in Fig. 5a and b, increasing the IMA and ERL concentrations caused a linear decrease in oxidation peaks of G and A, and the peak potential values shifted to more positive voltages for IMA and more negative voltages for ERL. The shifting in oxidation peak potentials of G and A peaks and the decrease in the peak currents may be attributed to the IMA's intercalative binding and the electrostatic

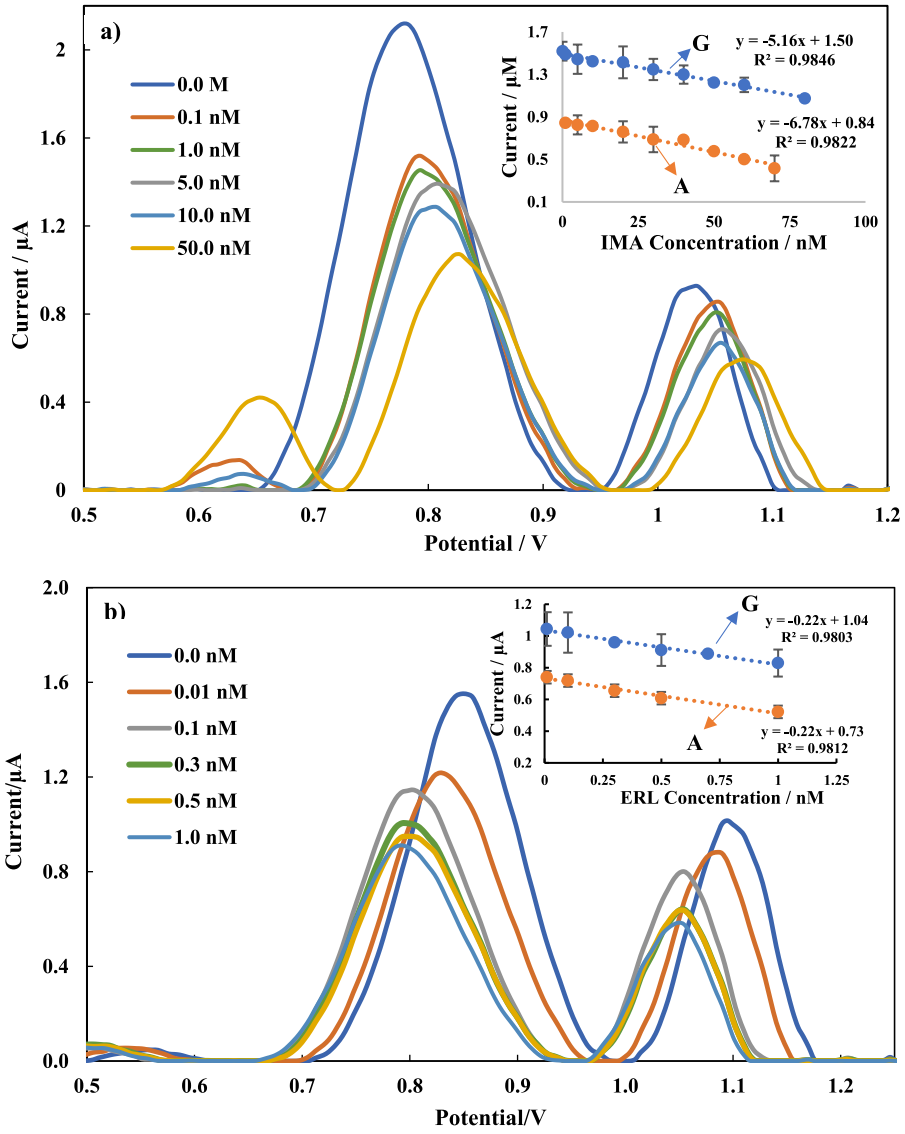

Fig. 5. DPVs of A and G with increasing concentrations of **a)** IMA **b)** ERL **Inset:** Plots of A and G peak current vs. IMA and ERL concentration (ABS, pH 4.8, E_{step}: 0.005 V, t_{pulse}: 0.07 s, scan rate: 0.025 V/s).

interaction of ERL to ds-DNA [37,38]. As seen from the voltammograms given in Fig. 5a, there is a third oxidation signal at about 0.65 V, which belongs to IMA and the related peak currents are parallel with the concentration of IMA. This peak does not interfere with DNA peaks.

Using these calibration studies, the performance parameters of the biosensor, namely linear working range, the limit of detection (LOD), the limit of quantification (LOQ), sensitivity, and reproducibility, were determined for both IMA and ERL using the conventional equations

Table 1
Validation parameters of DNA/AuPt/p-L-Met/SPE biosensor for IMA and ERL determination.

Validation parameters	IMA		ERL	
	A	G	A	G
Linear working range, nM	8.10–60	2.33–80	0.032–1.0	0.23–1.0
LOD, nM	2.40	0.18	0.009	0.07
LOQ, nM	8.10	2.33	0.032	0.23
Slope, µA/nM	6.78	5.16	0.22	0.22
Intercept, µA	0.84	1.50	0.73	1.04
Reproducibility, RSD%[a]	2.82	3.12	4.23	3.72

[a] Each value is the mean of five experiments.

LOD = 3 s/m and LOQ = 10 s/m, respectively. The results are given in Table 1.

In Table 2, LOD and linear working range data were compared with those reported for similar voltammetric studies of IMA and ERL in the literature. For IMA, the LOD value, 0.18 nM reached with the biosensor we developed, appears to be the best. Similarly, the LOD value for ERL, 0.009 nM, is lower than those given in previous reports.

To investigate the reproducibility of the electrode developed, the current signals of A and G were obtained from the interaction of 5 different sensors prepared with the same method with the same concentration of both IMA and ERL. The RSD% values obtained are given in Table 1. The fact that the calculated RSD% values for both substances are less than 5% indicates that the reproducibility of the biosensor is acceptable [51].

3.7. Interference study

To assess the biosensor's selectivity, the interference effects of several species common in pharmaceutical and biological samples (uric acid (UA), ascorbic acid (AA), glucose, L-glycine (L-Gly), Na_3PO_4, KCl, Ca^{2+}, and Mg^{2+}) were studied with a mole ratio of 1:1 were investigated.

Table 2
Comparison of the analytical performance of DNA/AuPt/p-L-Met/SPE biosensor with previously reported studies for IMA and ERL.

Method	Compound	Electrode	LOD, μM	Linear Working range, μM	Sample	Ref.
SWAdCS	IMA (reduction)	Dropping mercury electrode	0.0009–0.03	0.00026	Serum, urine and pharmaceutical preparation	[39]
SWV and SWAdCS	IMA (reduction)	Dropping mercury electrode	0.019–1.9	0.0056 (SWV) 0.0052 (AdsSWV)	Urine	[40]
DPV	IMA (oxidation)	GCE	–	0.00029	None	[41]
DPV	IMA (oxidation)	GCE	–	–	–	[42]
CV and DPV	IMA (mechanism studies)	GCE	–	–	–	[43]
DPV	IMA (oxidation)	pretreated BDDE	0.03–0.25	0.0063	Urine	[12]
DPV	IMA (oxidation)	HF/PGE	0.01–1 0.0 (1) 10.0–200.0 (2)	0.0074	Urine and serum	[44]
AdsSWV	IMA (oxidation)	MWCNT-COOH/SPCE	0.05–0.912	0.016	Urine	[1]
DPV	IMA (oxidation)	Fe_3O_4@MWCNTs@PANNFs/CPE	0.002–0.8500	0.0004	Urine	[45]
DPV	IMA	CuMOFs-MWCNTs/GCE	0.01–20.0 20.0–220.0	0.0041	Urine, serum and tablet	[46]
DPV	IMA	G/Ag/GCE	0.01–280.0	0.0011	Serum	[47]
HA and CV	IMA	Ni-NP/MCPE	4.0–400.0 1.0–38	1.2 0.35	Serum and tablet	[48]
AdsSWV	ERL	β-CD/GCE	0.01–8.0	0.0001	Pharmaceutical preparation	[49]
DPV	ERL ve CPT*	MWCNT-PUFIX/HF-PGE	0.11–23.50	0.02	Urine and nail	[50]
DPV	ERL	N-GQDs/CuNPs-PANI@GO/GRE	0.001–35.0	0.000712	Drug-injected aqueous solution, serum, and urine	[13]
DPV	***IMA***	***DNA/AuPt/p-L-Met/SPE***	*8.10-60 nM(A) 2.33-80 nM(G)*	*2.40nM (A) 0.18 nM (G)*	*Tablet and serum*	*Present work*
DPV	***ERL***	***DNA/AuPt/p-L-Met/SPE***	*0.032-1.0 nM (A) 0.23-1.0 nM(G)*	*0.009 nM (A) 0.07 nM (G)*	*Tablet and serum*	*Present work*

SWAdCS: Square Wave Adsorptive Cathodic Stripping Voltammetry; **SWV:** Square Wave Voltammetry; **DPV:** Differential Pulse Voltammetry; **CV:** Cyclic Voltammetry; **AdsSWV:** Adsorptive striping square wave voltammetry; **HA:** Hydrodynamic amperometry; **IMA:** Imatinib; **ERL:** Erlotinib; **CPT:** Capecitabine; **GCE:** Glassy carbon electrode; **Pretreated BDDE:** pretreated Boron doped diamond electrode; **HF/PGE:** Hollow fiber Pencil graphite electrode; **MWCNT-COOH/SPCE:** Multi-walled carbon nanotubes modified screen-printed carbon electrode; **Fe_3O_4@MWCNTs@PANNFs/CPE**: Fe_3O_4 nanoparticles supported on the multi-walled carbon nanotubes and polyacrylonitrile nanofiber modified carbon paste electrode; **CuMOFs-MWCNTs/GCE:** Metal–organic frameworks of copper and multiwall carbon nanotubes nanocomposite modified glassy carbon electrode; **G/Ag/GCE:** Graphene-Silver Nanocomposite modified glassy carbon electrode; **Ni-NP/MCPE:** Ni nanoparticle modified carbon paste electrode; **β-CD/GCE:** β-Cyclodextrin nanoparticles modified glassy carbon electrode; **MWCNT-PUFIX/HF-PGE:** Multivalued carbon nanotube—polyurethane/hollow fiber pencil graphite electrode; **N-GQDs/CuNPs-PANI@GO/GRE:** Nitrogen-doped graphene quantum dots and copper nanoparticles, polyaniline, along with graphene oxide modified graphite rod electrode; ***DNA/AuPt/p-L-Met/SPE**: DNA biosensor based on Au–Pt bimetallic nanoparticles and poly-L-methionine modified screen printed carbon electrode.*

The relative current differences (Δi_p%) obtained from the A and G oxidation signals before and after adding each species in the presence of IMA or ERL were given in Fig. S7.

$$\Delta i_p\% = \frac{i_0 - i_i}{i_0} \times 100$$

Here, i_0 represents the oxidation current value of A or G in the presence of IMA or ERL without any interferences and i_i represents the current value for A or G in the presence of 1:1 concentration of interferences with IMA or ERL.

The obtained results showed that the sensor was not significantly influenced by a 1:1 concentration of interferences.

3.8. Analytical application

To confirm the accuracy of the biosensor developed for IMA and ERL analysis, the tablet samples named GLIVEC containing IMA and TARCEVA containing ERL were analyzed with the DNA biosensor. The obtained recovery results are given in Table 3. These results indicate that the prepared biosensor can be utilized to determine IMA and ERL molecules with acceptable accuracy.

In order to test the applicability of the biosensor to biological samples, IMA and ERL determinations were also performed in human serum matrix, and the % recovery values were calculated and given in Table 4. The recovery results indicate that the proposed biosensor can be utilized to determine IMA and ERL molecules with satisfactory accuracy in biological samples.

Table 3
Recovery results in pharmaceutical samples.

A			G		
Added, nM	Found[a], nM	Average recovery[a], %	Added, nM	Found[a], nM	Average recovery[a], %
IMA (GLIVEC)					
5.0	4.8 ± 0.1	95.3 ± 3.9	5.0	5.1 ± 0.1	100.9 ± 1.8
ERL (TARCEVA)					
0.100	0.100 ± 0.002	100.3 ± 2.4	0.100	0.097	96.8 ± 1.7

[a] Each value is the mean of five experiments.

Table 4
Recovery results in human serum samples.

A			G		
Added, nM	Found[a], nM	Average recovery[a], %	Added, nM	Found[a], nM	Average recovery[a], %
IMA (serum)					
5.0	5.0 ± 0.04	100.6 ± 0.8	5.0	5.0 ± 0.1	101.2 ± 1.0
ERL (serum)					
0.100	0.099 ± 0.003	99.9 ± 2.7	0.100	0.097 ± 0.004	96.7 ± 3.8

[a] Each value is the mean of five experiments.

4. Conclusion

The current study developed a new, biocompatible, ultrasensitive electrochemical DNA biosensor based on poly-L-methionine and bimetallic AuPt nanoparticles to detect cancer therapy agents IMA and ERL. The interaction between IMA and ERL with ds-DNA onto the biosensor surface was utilized as a sensing process. The proposed DNA/AuPt/p-L-Met/SPE biosensor displayed remarkable catalytic and sensing processes for IMA and ERL determination in the concentration ranges of 2.33–80 nM and 0.032–1.0 nM, respectively. The obtained LOD values (0.18 nM for IMA and 0.009 nM for ERL) are the lowest among the comparable literature data. To confirm the accuracy and applicability of the biosensor developed, IMA and ERL analysis was performed on the tablet and human serum samples, and the results were satisfactory.

Credit authorship statement

Dilek Eskiköy Bayraktepe: Methodology, Writing-Original Draft, Funding acquisition, Resources, Investigation, Data curation. **Ceren Yıldız:** Investigation, Data curation, Methodology, and editing. **Zehra Yazan:** Supervision, Investigation, Conceptualization, Writing – review & editing.

Declaration of competing interest

The authors declare that they have no known competing financial interests or personal relationships that could have appeared to influence the work reported in this paper.

Data availability

Data will be made available on request.

Acknowledgments

The authors are highly thankful to The Scientific and Technological Research Council of Turkey (TUBITAK) and Ankara University Research Fund from Turkey for the financial support with project numbers 120Z912 and 20L0430001, respectively.

Appendix A. Supplementary data

Supplementary data to this article can be found online at https://doi.org/10.1016/j.talanta.2023.124361.

References

[1] J. Rodríguez, G. Castañeda, I. Lizcano, Electrochemical sensor for leukemia drug imatinib determination in urine by adsorptive striping square wave voltammetry using modified screen-printed electrodes, Electrochim. Acta 269 (2018) 668–675, https://doi.org/10.1016/j.electacta.2018.03.051.

[2] V.M. Rezende, A.J. Rivellis, M.M. Gomes, F.A. Dörr, M.M.Y. Novaes, L. Nardinelli, A.L.d.L. Costa, D.d.A.F. Chamone, I. Bendit, Determination of serum levels of imatinib mesylate in patients with chronic myeloid leukemia: validation and application of a new analytical method to monitor treatment compliance, Rev. Bras. Hematol. Hemoter. 35 (2013) 103–108, https://doi.org/10.5581/1516-8484.20130030.

[3] D.R. Gandara, B. Piperdi, W.V. Walsh, A Randomized Phase II Study of Schedule-Modulated Concomitant Pemetrexed (Alimta®) and Erlotinib (Tarceva®) vs Single Agent Pemetrexed (Alimta®) in Patients with Progressive or Recurrent Non-small Cell Lung Cancer (NSCLC).

[4] I. Bulur, Z.N. Saraçoglu, E. Böyük, F. Canaz, A case of imatinib-induced erythrodermia, Turkderm Turk. Arch. Dermatol. Venereol. 48 (2014) 54, https://doi.org/10.4274/turkderm.02223.

[5] O. Fiala, P. Hosek, M. Pesek, J. Finek, J. Racek, P. Stehlik, O. Sorejs, M. Minarik, L. Benesova, A. Celer, Serum concentration of erlotinib and its correlation with outcome and toxicity in patients with advanced-stage NSCLC, Anticancer Res. 37 (2017) 6469–6476, https://doi.org/10.21873/anticanres.12102.

[6] K. Titier, S. Picard, D. Ducint, E. Teilhet, N. Moore, P. Berthaud, F.-X. Mahon, M. Molimard, Quantification of imatinib in human plasma by high-performance liquid chromatography-tandem mass spectrometry, Ther. Drug Monit. 27 (2005) 634–640, https://doi.org/10.1097/01.ftd.0000175973.71140.91.

[7] C. Singh, S. Verma, A. Singh, R. Jha, O. Porwal, N. Fuloria, P. Sharma, Development and validation of stability indicating high performance liquid chromatography method for related substances of imatinib mesylate, Indian J. Pharmaceut. Sci. 84 (2022) 465–476, https://doi.org/10.36468/pharmaceutical-sciences.940.

[8] R. Reis, L. Labat, M. Allard, P. Boudou-Rouquette, J. Chapron, A. Bellesoeur, A. Thomas-Schoemann, J. Arrondeau, F. Giraud, J. Alexandre, Liquid chromatography-tandem mass spectrometric assay for therapeutic drug monitoring of the EGFR inhibitors afatinib, erlotinib and osimertinib, the ALK inhibitor crizotinib and the VEGFR inhibitor nintedanib in human plasma from non-small cell lung cancer patients, J. Pharm. Biomed. Anal. 158 (2018) 174–183, https://doi.org/10.1016/j.jpba.2018.05.052.

[9] T. Khuroo, U. Atifa, A. Khuroo, M.A. Mirza, A. Ali, Z. Iqbal, Simultaneous estimation of Paclitaxel and Erlotinib in plasma by liquid chromatography/(+) electrospray tandem mass spectrometry: application in formulation development and pharmacokinetics, Drug Dev. Ind. Pharm. (2022) 1–25, https://doi.org/10.1080/03639045.2022.2108830.

[10] R. Rathod, L. Rathod, A. Mundada, H. Patel, Validated UV spectrophotometric methods for the determination of anticancer drug erlotinib hydrochloride in bulk and tablet formulations, J. Appl. Spectrosc. 88 (2021) 882–886, https://doi.org/10.1007/s10812-021-01254-9.

[11] R.S. Sri, K.B. Sri, M. Sumakanth, Stability indicating UV-Spectrophotometric method development and its validation for the determination of imatinib mesylate in bulk and formulation, Asian J. Pharm. Anal. 12 (2022) 83–86, https://doi.org/10.52711/2231-5675.2022.00015.

[12] M. Brycht, K. Kaczmarska, B. Uslu, S.A. Ozkan, S. Skrzypek, Sensitive determination of anti-cancer drug imatinib in spiked human urine samples by differential pulse voltammetry on anodically pretreated boron-doped diamond electrode, Diam. Relat. Mater. 68 (2016) 13–22, https://doi.org/10.1016/j.diamond.2016.05.007.

[13] H. Rahmanian, Z. Es' haghi, M. Dadmehr, A robust electrochemical sensing platform for the detection of erlotinib based on nitrogen-doped graphene quantum dots/copper nanoparticles-polyaniline-graphene oxide nanohybrid, Nanotechnology 34 (2022), 015502, https://doi.org/10.1088/1361-6528/ac8996.

[14] M. Pohanka, P. Skládal, Electrochemical biosensors-principles and applications, J. Appl. Biomed. 6 (2008) 57–64, https://doi.org/10.32725/jab.2008.008.

[15] N.J. Ronkainen, H.B. Halsall, W.R. Heineman, Electrochemical biosensors, Chem. Soc. Rev. 39 (2010) 1747–1763, https://doi.org/10.1039/B714449K.

[16] J.L. Hammond, N. Formisano, P. Estrela, S. Carrara, J. Tkac, Electrochemical biosensors and nanobiosensors, Essays Biochem. 60 (2016) 69–80, https://doi.org/10.1042/EBC20150008.

[17] H. Karimi-Maleh, M. Alizadeh, Y. Orooji, F. Karimi, M. Baghayeri, J. Rouhi, S. Tajik, H. Beitollahi, S. Agarwal, V.K. Gupta, Guanine-based DNA biosensor amplified with Pt/SWCNTs nanocomposite as analytical tool for nanomolar determination of daunorubicin as an anti-cancer drug: a docking/experimental investigation, Ind. Eng. Chem. Res. 60 (2021) 816–823, https://doi.org/10.1021/acs.iecr.0c04698.

[18] H.R.A. Hasanjani, K. Zarei, An electrochemical sensor for attomolar determination of mercury (II) using DNA/poly-L-methionine-gold nanoparticles/pencil graphite electrode, Biosens. Bioelectron. 128 (2019) 1–8, https://doi.org/10.1016/j.bios.2018.12.039.

[19] V. Kavita, DNA biosensors-a review, J. Bioeng Biomed. Sci. 7 (2017) 222, https://doi.org/10.4172/2155-9538.1000222.

[20] A. Liu, K. Wang, S. Weng, Y. Lei, L. Lin, W. Chen, X. Lin, Y. Chen, Development of electrochemical DNA biosensors, TrAC, Trends Anal. Chem. 37 (2012) 101–111, https://doi.org/10.1016/j.trac.2012.03.008.

[21] A. Erdem, M. Ozsoz, Electrochemical DNA biosensors based on DNA-drug interactions, Electroynalysis (N.Y.N.Y.) 14 (2002) 965–974, https://doi.org/10.1002/1521-4109(200208)14:14<965::AID-ELAN965>3.0.CO;2.

[22] R. Couto, J. Lima, M. Quinaz, Recent developments, characteristics and potential applications of screen-printed electrodes in pharmaceutical and biological analysis, Talanta 146 (2016) 801–814, https://doi.org/10.1016/j.talanta.2015.06.011.

[23] J.M. George, A. Antony, B. Mathew, Metal oxide nanoparticles in electrochemical sensing and biosensing: a review, Microchim. Acta 185 (2018) 1–26, https://doi.org/10.1007/s00604-018-2894-3.

[24] M. Pumera, Voltammetry of carbon nanotubes and graphenes: excitement, disappointment, and reality, Chem. Rec. 12 (2012) 201–213, https://doi.org/10.1002/tcr.201100027.

[25] H.K. Kordasht, M. Hasanzadeh, F. Seidi, P.M. Alizadeh, Poly (amino acids) towards sensing: recent progress and challenges, TrAC, Trends Anal. Chem. 140 (2021), 116279, https://doi.org/10.1016/j.trac.2021.116279.

[26] Z. Navrátilová, P. Kula, Clay modified electrodes: present applications and prospects, Electroynalysis (N.Y.N.Y.) 15 (2003) 837–846, https://doi.org/10.1002/elan.200390103.

[27] M.R. de Barros, J.P. Winiarski, W.C. Elias, C.E.M. de Campos, C.L. Jost, Au-on-Pd bimetallic nanoparticles applied to the voltammetric determination and monitoring of 4-nitroaniline in environmental samples, J. Environ. Chem. Eng. 9 (2021), 105821, https://doi.org/10.1016/j.jece.2021.105821.

[28] S. Sawan, R. Maalouf, A. Errachid, N. Jaffrezic-Renault, Metal and metal oxide nanoparticles in the voltammetric detection of heavy metals: a review, TrAC, Trends Anal. Chem. 131 (2020), 116014, https://doi.org/10.1016/j.trac.2020.116014.

[29] H.R.A. Hasanjani, K. Zarei, DNA/Au-Pt bimetallic nanoparticles/graphene oxide-chitosan composites modified pencil graphite electrode used as an electrochemical biosensor for sub-picomolar detection of anti-HIV drug zidovudine, Microchem. J. 164 (2021), 106005, https://doi.org/10.1016/j.microc.2021.106005.

[30] Z. Wang, J. Li, L. Xu, Y. Feng, X. Lu, Electrochemical sensor for determination of aflatoxin B1 based on multiwalled carbon nanotubes-supported Au/Pt bimetallic nanoparticles, J. Solid State Electrochem. 18 (2014) 2487–2496, https://doi.org/10.1007/s10008-014-2506-z.
[31] E.S. Gomes, F.R. Leite, B.R. Ferraz, H.A. Mourao, A.R. Malagutti, Voltammetric sensor based on cobalt-poly (methionine)-modified glassy carbon electrode for determination of estriol hormone in pharmaceuticals and urine, J. Pharm. Anal. 9 (2019) 347–357, https://doi.org/10.1016/j.jpha.2019.04.001.
[32] G. Venkataprasad, T.M. Reddy, P. Shaikshavali, P. Gopal, A novel electrochemical sensor based on multi-walled carbon nanotubes/poly (L-Methionine) for the investigation of 5-Nitroindazole: a voltammetric study, Anal. Chem. Lett. 8 (2018) 457–474, https://doi.org/10.1080/22297928.2018.1479304.
[33] T. Hezard, K. Fajerwerg, D. Evrard, V. Collière, P. Behra, P. Gros, Gold nanoparticles electrodeposited on glassy carbon using cyclic voltammetry: application to Hg (II) trace analysis, J. Electroanal. Chem. 664 (2012) 46–52, https://doi.org/10.1016/j.jelechem.2011.10.014.
[34] G. Lu, G. Zangari, Electrodeposition of platinum on highly oriented pyrolytic graphite. Part I: electrochemical characterization, J. Phys. Chem. B 109 (2005) 7998–8007, https://doi.org/10.1021/jp0407324.
[35] C. Liu, D. Jiang, G. Xiang, L. Liu, F. Liu, X. Pu, An electrochemical DNA biosensor for the detection of Mycobacterium tuberculosis, based on signal amplification of graphene and a gold nanoparticle–polyaniline nanocomposite, Anlst 139 (2014) 5460–5465, https://doi.org/10.1039/C4AN00976B.
[36] A.A. Ensafi, M. Amini, B. Rezaei, Biosensor based on ds-DNA decorated chitosan modified multiwall carbon nanotubes for voltammetric biodetection of herbicide amitrole, Colloids Surf. B Biointerfaces 109 (2013) 45–51, https://doi.org/10.1016/j.colsurfb.2013.03.031.
[37] M. Pešić, J. Bugarinović, A. Minić, S.B. Novaković, G.A. Bogdanović, A. Todosijević, D. Stevanović, I. Damljanović, Electrochemical characterization and estimation of DNA-binding capacity of a series of novel ferrocene derivatives, Bioelectrochemistry 132 (2020), 107412, https://doi.org/10.1016/j.bioelechem.2019.107412.
[38] D.E. Bayraktepe, A voltammetric study on drug-DNA interactions: kinetic and thermodynamic aspects of the relations between the anti-cancer agent dasatinib and ds-DNA using a pencil lead graphite electrode, Microchem. J. 157 (2020), 104946, https://doi.org/10.1016/j.microc.2020.104946.
[39] E. Hammam, H. El-Desoky, A. Tawfik, M. Ghoneim, Voltammetric behavior and quantification of the anti-leukemia drug imatinib in bulk form, pharmaceutical formulation, and human serum at a mercury electrode, Can. J. Chem. 82 (2004) 1203–1209, https://doi.org/10.1139/v04-060.
[40] J. Rodriguez, J. Berzas, G. Castaneda, N. Rodriguez, Voltammetric determination of Imatinib (Gleevec) and its main metabolite using square-wave and adsorptive stripping square-wave techniques in urine samples, Talanta 66 (2005) 202–209, https://doi.org/10.1016/j.talanta.2004.11.010.
[41] V.C. Diculescu, M. Vivan, A.M.O. Brett, Voltammetric behavior of antileukemia drug glivec. Part I–electrochemical study of glivec, Electroynalysis (N.Y.N.Y.) 18 (2006) 1800–1807, https://doi.org/10.1002/elan.200603591.
[42] V.C. Diculescu, M. Vivan, A.M.O. Brett, Voltammetric behavior of antileukemia drug glivec. Part II–redox processes of glivec electrochemical metabolite, Electroynalysis (N.Y.N.Y.) 18 (2006) 1808–1814, https://doi.org/10.1002/elan.200603592.
[43] V.C. Diculescu, M. Vivan, A.M.O. Brett, Voltammetric behavior of antileukemia drug glivec. Part III: in situ DNA oxidative damage by the glivec electrochemical metabolite, Electroynalysis (N.Y.N.Y.) 18 (2006) 1963–1970, https://doi.org/10.1002/elan.200603602.
[44] B. Hatamluyi, Z. Es' haghi, A layer-by-layer sensing architecture based on dendrimer and ionic liquid supported reduced graphene oxide for simultaneous hollow-fiber solid phase microextraction and electrochemical determination of anti-cancer drug imatinib in biological samples, J. Electroanal. Chem. 801 (2017) 439–449, https://doi.org/10.1016/j.jelechem.2017.08.032.
[45] M. Ghapanvari, T. Madrakian, A. Afkhami, A. Ghoorchian, A modified carbon paste electrode based on Fe3O4@ multi-walled carbon nanotubes@ polyacrylonitrile nanofibers for determination of imatinib anti-cancer drug, J. Appl. Electrochem. 50 (2020) 281–294, https://doi.org/10.1007/s10800-019-01388-x.
[46] B.H. Pour, N. Haghnazari, F. Keshavarzi, E. Ahmadi, B.R. Zarif, High sensitive electrochemical sensor for imatinib based on metal-organic frameworks and multiwall carbon nanotubes nanocomposite, Microchem. J. 165 (2021), 106147, https://doi.org/10.1016/j.microc.2021.106147.
[47] Z. Wu, J. Liu, M. Liang, H. Zheng, C. Zhu, Y. Wang, Detection of imatinib based on electrochemical sensor constructed using biosynthesized graphene-silver nanocomposite, Front. Chem. 9 (2021), 670074, https://doi.org/10.3389/fchem.2021.6700.
[48] F. Khakpoor, S. Fathi, Electrocatalytic determination of anti-cancer drug imatinib, using Ni nanoparticle modified carbon paste electrode, JACR 15 (2021) 67–78, 20.1001.1.20083815.2021.15.4.6.1.
[49] N.K. Bakirhan, T.T. Tok, S.A. Ozkan, The redox mechanism investigation of non-small cell lung cancer drug: erlotinib via theoretical and experimental techniques and its host–guest detection by β-Cyclodextrin nanoparticles modified glassy carbon electrode, Sensor. Actuator. B Chem. 278 (2019) 172–180, https://doi.org/10.1016/j.snb.2018.09.090.
[50] Z. Es' haghi, F. Moeinpour, Carbon nanotube/polyurethane modified hollow fiber-pencil graphite electrode for in situ concentration and electrochemical quantification of anti-cancer drugs Capecitabine and Erlotinib, Eng. Life Sci. 19 (2019) 302–314, https://doi.org/10.1002/elsc.201800167.
[51] J. Wang, X. Yi, H. Tang, H. Han, M. Wu, F. Zhou, Direct quantification of microRNA at low picomolar level in sera of glioma patients using a competitive hybridization followed by amplified voltammetric detection, Anal. Chem. 84 (2012) 6400–6406, https://doi.org/10.1021/ac203368h.